Nonequilibrium quasiparticle relaxation dynamics in single crystals of hole- and electron-doped $BaFe_2As_2$

Darius H. Torchinsky,[1] James W. McIver,[1] David Hsieh,[1] G. F. Chen,[2] J. L. Luo,[2] N. L. Wang,[2] and Nuh Gedik[1,*]

[1]*Department of Physics, Massachusetts Institute of Technology, Cambridge, Massachusetts, 02139, USA*

[2]*Beijing National Laboratory for Condensed Matter Physics, Institute of Physics, Chinese Academy of Sciences, Beijing 100190, China*

(Received 11 February 2011; revised manuscript received 3 June 2011; published 13 September 2011)

We report on the nonequilibrium quasiparticle dynamics in $BaFe_2As_2$ on both the hole-doped ($Ba_{1-x}K_xFe_2As_2$) and electron-doped ($BaFe_{2-y}Co_yAs_2$) sides of the phase diagram using ultrafast pump-probe spectroscopy. Below T_c, measurements conducted at low photoinjected quasiparticle densities in the optimally and overdoped $Ba_{1-x}K_xFe_2As_2$ samples reveal two distinct relaxation processes: a fast component whose decay rate increases linearly with excitation density and a slow component with an excitation density independent decay rate. We argue that these two processes reflect the recombination of quasiparticles in the two hole bands through intraband and interband processes. We also find that the thermal recombination rate of quasiparticles increases quadratically with temperature in these samples. The temperature and excitation density dependence of the decays indicates fully gapped hole bands and nodal or very anisotropic electron bands. At higher excitation densities and lower hole dopings, the dependence of the dynamics on quasiparticle density disappears as the data are more readily understood in terms of a model which accounts for the quasiequilibrium temperature attained by the sample. In the $BaFe_{2-y}Co_yAs_2$ samples, dependence of the recombination rate on quasiparticle density at low dopings (i.e., $y = 0.12$) is suppressed upon submergence of the inner hole band and quasiparticle relaxation occurs in a slow, density-independent manner.

DOI: 10.1103/PhysRevB.84.104518 PACS number(s): 74.25.Gz, 78.47.jh

I. INTRODUCTION

The discovery of the iron-pnictide superconductors[1,2] has opened a new chapter in the study of high-temperature superconductivity. Although they display a lower degree of electronic correlation than the cuprates,[3] there are a number of similarities between the two material classes. Perhaps the most striking of these is the close correspondence between their phase diagrams. In both classes, superconductivity is achieved by the doping of either electrons or holes into a "parent" material which displays magnetic ordering at lower temperatures, i.e., spin density wave (SDW) ordering in the pnictides[4,5] or antiferromagnetic ordering in the cuprates. As this static magnetic ordering is suppressed with doping, superconductivity emerges, increasing in transition temperature T_c to a maximum at optimal doping before receding with the addition of further carriers.

With these shared characteristics come shared mysteries, including the natures of the pseudogap state, of the coexistence between magnetic and superconducting order (i.e., homogeneous vs heterogeneous), and, arguably the most fundamental, the binding boson itself. The presence of a resonance in neutron scattering spectra below T_c in the pnictides[6,7] and the suppression of magnetic ordering upon the addition of carriers suggest that antiferromagnetic spin fluctuations mediate pairing, implying that the superconducting order parameter Δ switches sign in the Brillouin zone. Therefore, definitive determination of the gap structure and symmetry would serve as a significant step toward understanding the mechanism of superconductivity. In the cuprates, experiments clearly show d-wave pairing.[8] The picture in the pnictides is a lot murkier, in part due to their multiband character and the fact that interband interactions likely play a role in superconductivity.[9–11] This complexity may be at the origin of the seemingly conflicting sets of experimental evidence concerning the symmetry of Δ. Angle-resolved photoemission (ARPES) studies have consistently revealed a fully gapped Fermi surface,[12–14] while NMR[15] and magnetic-penetration-depth[16] measurements suggest the presence of nodes. Confronted with these data, theorists have proposed a diverse collection of order parameters, including an $s_\pm$ symmetry with nodes,[17] d_{xy} symmetry,[18] and the prevailing nodeless $s_\pm$ order parameter[9] with interband impurity scattering.[11]

In this paper we use optical pump-probe spectroscopy to investigate the gap symmetry and interband interactions in the Ba-122 system of the iron pnictides. Pump-probe spectroscopy is a powerful technique in which absorption of an ultrashort "pump" pulse results in the injection of a transient population density n of nonequilibrium quasiparticles.[19] A second "probe" pulse then records the return of the system to equilibrium through measurement of the time-resolved change in reflectivity $\Delta R(t)/R$, assumed linearly proportional to n. These measurements have been successfully employed in the cuprates to examine, e.g., gap symmetry[20,21] and the strength of electron-boson coupling.[22,23] In the pnictides, pump-probe spectroscopy has probed the existence of a pseudogap state,[24] the competition between SDW and superconducting ordering,[25] coherent lattice vibrations to rule out their role in superconductivity,[26] and the role of interband interactions and gap symmetry in nonequilibrium quasiparticle relaxation.[27] As prior ultrafast experiments have focused on one side of the phase diagram at a time, there is a need for a systematic study of the pnictides as a function of doping across the phase diagram.

Building upon our prior work,[27] we study both the hole-doped $Ba_{1-x}K_xFe_2As_2$ and the electron-doped $BaFe_{2-y}Co_yAs_2$ series of the 122 pnictides. In the optimal to overdoped hole-doped samples ($x = 0.4, 0.5, 0.6$), the signal $\Delta R(t)/R$ is composed of two distinct features. The first is a fast

component whose decay rate depends on excitation fluence Φ, which, aided by ARPES[12,14,28] measurements and local density approximation (LDA) calculations,[29] we argue arises from the inner hole bands. The second is a slow, fluence-independent decay we attribute to the outer hole band. An analysis of the fast component based on the Rothwarf-Taylor[20,30] coupled differential equations reveals a T^2 dependence of the thermal population of quasiparticles on temperature, suggesting the presence of nodes on the Fermi surface. At the same time, the number of photoinduced quasiparticles that contribute to the overall signal increases linearly with laser fluence, reflecting the fully gapped character of these bands. We thus argue that these observations are consistent with fully gapped hole pockets at the zone center and nodal or highly anisotropic electron pockets at the zone boundary.

In the normal state we observe oscillations in the reflectivity transients due to coherent acoustic phonons. These thermally driven acoustic waves are suppressed below T_c due to a significant decrease in the thermal expansion coefficient below the transition,[31–33] except at the highest fluences, suggesting a dichotomy between the low- and high-fluence regimes.

These arguments provide a framework for understanding the rest of the available phase diagram. At lower hole doping levels (i.e., $x = 0.2$, $x = 0.3$) and higher excitation fluences, the data represent the normal-state behavior seen at higher dopings. In the low-fluence regime, however, these samples do not exhibit the density-dependent recombination seen for the optimally and overdoped samples, precluding an analysis to determine Fermi surface topology. Rather, these data are qualitatively explained by a simple model that accounts for the spatially integrated nature of the pump-probe measurement.

In the Co-doped samples, low-fluence measurements below T_c in an underdoped ($y = 0.12$) sample indicate quasiparticle recombination that is weakly dependent on incident fluence. This intensity-dependent recombination disappears as further electron doping submerges the innermost hole pocket below the Fermi level; for large values of Co doping, the only observed relaxation is the slow decay we previously assigned to the outer hole band.

II. EXPERIMENTAL SETUP

We employed a Ti:sapphire oscillator system which produces 60-fs pulses at central wavelength 795 nm (photon energy 1.5 eV) at an 80-MHz repetition rate. After passing through a prism compressor designed to account for the dispersion of the setup, the repetition rate of the laser was reduced to 1.6 MHz with an electro-optic pulse picker in order to eliminate the effects of cumulative heating of the sample. The beam was then split into two paths with a 9:1 ratio between the pump and probe. The horizontally polarized pump beam was chopped at 102 kHz by a photoelastic modulator/polarizer pair for lock-in detection and then passed through neutral density filters in order to tune the incident pump fluence from 44 μJ/cm^2 to 44 nJ/cm^2. After attenuation, the pump beam was passed through a fast scanning delay stage which swept the pump delay by ~40 ps at a rate of 30 Hz before being focused to a 60 μm FWHM spot size on the sample.

After being split from the pump, the probe beam passed through a computer-controlled motorized delay stage and was rotated to vertical polarization before being focused to a 60-μm FWHM spot size on the sample in the same location as the pump. The reflected probe beam was separated from the pump by spatial and polarization filtering, then focused onto a photodiode. The photodiode output was low-pass filtered and measured by a lock-in amplifier synched with the photoelastic modulator. We used a fast time constant (30 μs) so that the lock-in output could be input to an oscilloscope triggered to the fast-scanning stage. We averaged several fast-scan stage sweeps to record each data trace.

All samples were grown using the self-flux method in proportions given by their chemical formula. A variety of sample characterization methods were employed, with the most rigorous testing reserved for the optimally hole-doped ($x = 0.4$) sample as follows: the induction-coupled plasma (ICP) technique was used to determine the Ba/K ratio, the uncertainty of which was determined to be less than 2%.[34] Energy-dispersive x-ray (EDX) spectroscopy was used to determine spatial variation in sample doping homogeneity. A plot of the resulting EDX analysis pattern may be found in Fig. 1(b) of Ref. 34. In a recent EDX analysis on a different batch of samples, the maximum spatial variation was found to range from $x = 0.39$ to $x = 0.44$. Resistivity and magnetic susceptibility measurements have been independently performed and presented;[14] the sharpness of the transition was used as a gauge of sample purity. These results are shown in Figs. 1(a) and 1(b) of Ref. 14.

A number of other studies on samples from the same batch of optimally hole-doped compounds have been performed, including ARPES,[12,14,28] infrared spectroscopy,[35] and thermal conductivity;[36] further information regarding sample purity and homogeneity may be found therein. We performed superconducting quantum interference device (SQUID) magnetometry on all the samples used in this study and measured transition width $\Delta T_c \sim 1$ K at each sample's transition temperature.

III. RESULTS AND DISCUSSION

A schematic representation of the Ba-122 phase diagram is presented in Fig. 1. The data points indicate the T_c and T_{SDW} values for the samples used in this study. Specifically, we examined hole-doped $Ba_{1-x}K_xFe_2As_2$ with $x = 0.2 - 0.6$ in increments of 0.1, spanning the regime from underdoping to overdoping. On the electron-doped side of the phase diagram, we studied $BaFe_{2-y}Co_yAs_2$ samples at doping levels of $y = 0.08 - 0.20$ in increments of 0.04, which spans underdoped to optimally doped samples. The parent compound was also measured.

We start by describing our measurements in $Ba_{1-x}K_xFe_2As_2$ in the optimally ($x = 0.4$) to overdoped ($x = 0.6$) regime at the low excitation densities. Shifting our attention to the high-fluence regime provides a framework for measurements in the underdoped ($x = 0.2$,0.3) samples, which we follow with a discussion of measurements in the parent compound and $BaFe_{2-x}Co_xAs_2$ at all dopings.

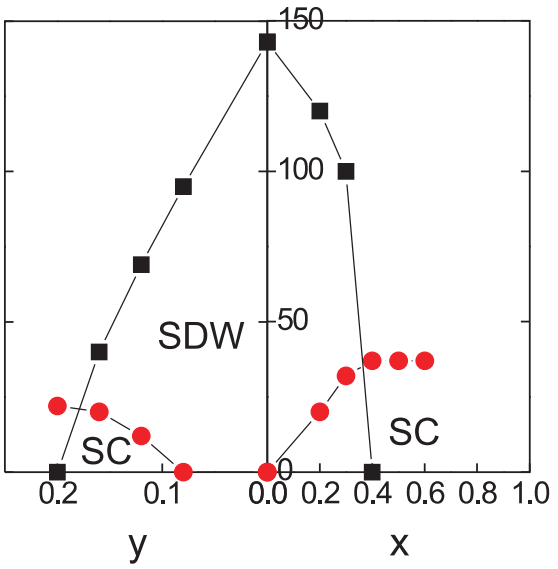

FIG. 1. (Color online) Schematic phase diagram of the Ba-122 pnictides for the hole-doped $Ba_{1-x}K_xFe_2As_2$ and electron-doped $BaFe_{2-y}Co_yAs_2$ samples used in this study. The T_c values are denoted by black squares and the T_{SDW} values are given by red circles. All T_c values were measured by SQUID magnetometry. The values for T_{SDW} on the electron-doped side of the phase diagram were determined from the same batch of samples,[37] while the values for T_{SDW} on the hole-doped side of the phase diagram are from the literature.[38]

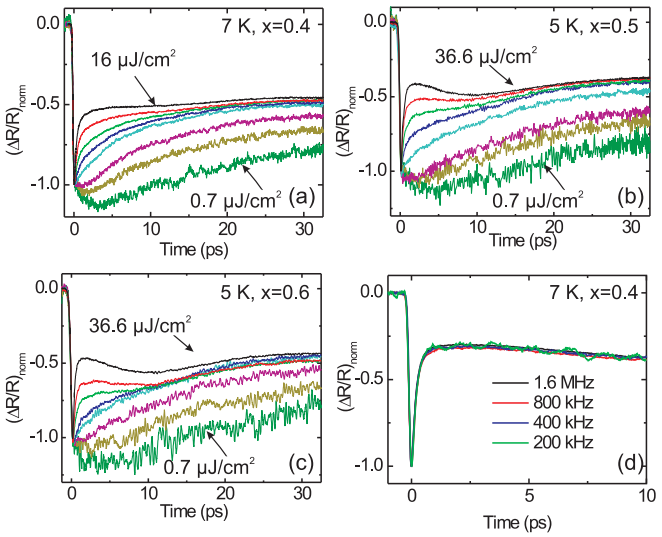

FIG. 2. (Color online) Fast, intensity-dependent relaxation of the normalized reflectivity transients $(\Delta R/R)_{norm}$ in the superconducting state. (a) The decay rate of $[\Delta R(t)/R]_{norm}$ in the optimally doped compound ($x = 0.4$) systematically decreases with decreasing intensity at 7 K [from bottom to top: $\Phi = 0.7$ μJ/cm^2 (light green), 2.2, 4.4, 7.0, 8.9, 12.8, to 16.1 μJ/cm^2 (black)]. Raw traces from the overdoped hole-doped samples $Ba_{1-x}K_xFe_2As_2$ for (b) $x = 0.5$ and (c) $x = 0.6$ at $T = 5$ K are qualitatively identical to those for the optimally doped sample in panel (a). In both of these plots, the absorbed fluences are, from bottom to top, $\Phi = 0.7$ μJ/cm^2 (blue), 1.4, 2.2, 4.4, 7.0, 12.7, 20.1, and 36.6 μJ/cm^2 (black). (d) $(\Delta R/R)_{norm}$ measured at four different repetition rates are identical, verifying the absence of cumulative heating ($\Phi = 37$ μJ/cm^2, $T = 7$ K).

A. $Ba_{1-x}K_xFe_2As_2$: The low-fluence regime

Characteristic short-time traces of the normalized change in reflectivity $\Delta R/R$ as a function of time at various fluences Φ are shown in Fig. 2(a) for the $x = 0.4$ sample at $T = 7$ K. There is an initial decrease of the reflectivity at the arrival of the pump beam at time $t = 0$. Recovery to equilibrium depends strongly on the incident fluence, with higher fluences exhibiting a faster initial relaxation rate than lower ones. Qualitatively identical intensity dependence is observed in the $x = 0.5, 0.6$ samples, as shown in Figs. 2(b) and 2(c). In all cases, higher fluences are marked by faster initial relaxation of the signal than for lower fluences. We note the presence of the beginning of a heavily damped oscillation in the highest fluences of this figure (not shown for the $x = 0.4$ sample, although it is was observed) due to stimulated Brillouin scattering (SBS), which disappears with decreasing fluence. This characteristic of the data is described in further detail below, within the context of the high-fluence regime measurements.

In order to rule out steady-state heating as the source of this intensity dependence, we used a pulse picker to vary the repetition rate. Figure 2(d) shows $T = 7$ K transients taken with an absorbed pump fluence $\Phi = 37$ μJ/cm^2 at repetition rates ranging from 200 kHz to 1.6 MHz. We observe no discernible change in the recovery dynamics. Measurements performed above T_c exhibited an absence of the intensity dependence of Figs. 2(a)–2(c), verifying its origin in superconductivity.[27]

The reflectivity transients of Figs. 2(a)–2(c) tend to an offset at the end of the 30 ps measurement time window. This offset is the beginning of a slow, intensity-independent decay with a characteristic decay time of ~500 ps,[27] represented for the $x = 0.4$ sample at 7 K by the black trace in Fig. 3(a). As with the fast, intensity-dependent component, the slowly decreasing offset is observed to abruptly shut off for all samples at their respective transition temperatures, leading to a much longer decay of lower magnitude, as seen in the red trace of Fig. 3(a). This switching off of the long-time component was also a universal characteristic of the $x = 0.4 - 0.6$ samples, which is demonstrated by Figs. 3(b)–3(d).

Further insight into the data is obtained by considering the initial amplitude of the reflectivity transients. Figure 4(a) presents $\Delta R(0)/R$ as a function of the absorbed pump fluence in the low-fluence regime at $T = 7$ K in the $x = 0.4 - 0.6$ samples. Lines of slope 1 are shown with the data, indicating that at these fluences, $\Delta R(0)/R \propto n_0$ is directly proportional to Φ. This linear proportionality signifies that these experiments represent the low-fluence regime. Significantly, a linear dependence of n_0 on Φ is an indication that the photoinduced excitations are fully gapped; the number of excitations is simply proportional to the laser energy absorbed.[20] In the presence of a line node in the gap of the probed excitations, a linear dependence of the density of states $g(E)$ on energy E produces an estimate for the total energy absorbed by the quasiparticles as $E_T \sim \int g(E)EdE \sim E^3$. In such a case, the total number of excited quasiparticles n_{ph} is given as $n_{ph} \sim \int g(E)dE \sim E^2$. Thus the number of photoinduced quasiparticles in terms of the energy deposited is given as $n_{ph} \sim E_T^{2/3}$, implying that a line node in the vicinity of the photoexcited quasiparticles

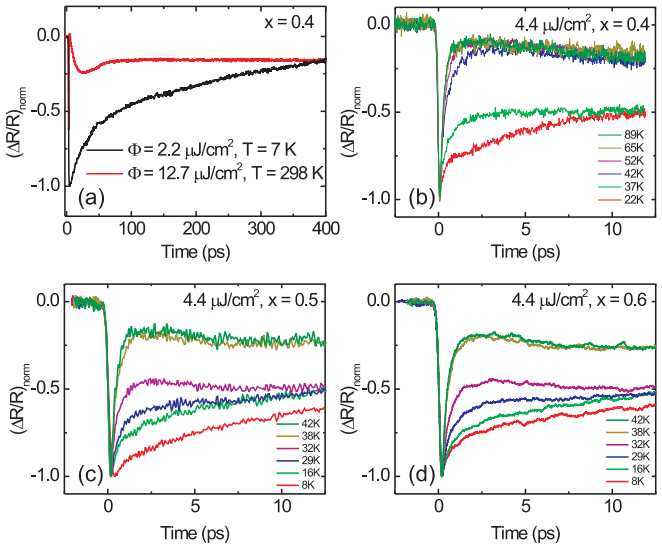

FIG. 3. (Color online) Slow relaxation of $(\Delta R/R)_{\rm norm}$ in the superconducting state. (a) $(\Delta R/R)_{\rm norm}$ at 7 K and at room temperature. The slow, excitation-density-independent portion (black) switches off to become a nearly flat response in the normal state, which clearly shows the first oscillation due to stimulated Brillouin scattering. (b–d) A more complete view of the temperature dependence of $(\Delta R/R)_{\rm norm}$ near T_c obtained at $\Phi = 4.4$ J/cm^2 in the $x = 0.4 - 0.6$ samples. We note a sharp decrease in the offset across the transition (i.e., 37 to 42 K) due to switching off of the long-time component with loss of superconductivity. Above T_c there is an upturn of the signal evident at short times due to stimulated Brillouin scattering.[39]

should yield a sublinear dependence of the initial reflectivity transients $\Delta R(0)/R \propto \Phi^{2/3}$, which is not observed.

With increasing Φ, $\Delta R(0)/R$ displays saturation behavior at high excitation densities, as seen for the $x = 0.4$, $T = 7$ K data in Fig. 4(b). We fit these data to a simple saturation model which accounts for the exponential penetration of the light into

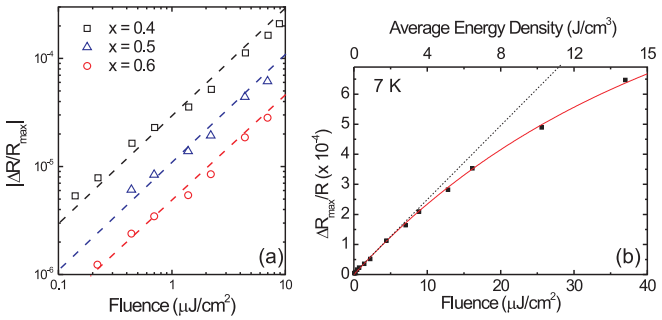

FIG. 4. (Color online) (a) $|(\Delta R/R)_{\rm max}|$ plotted as a function of Φ at $T = 7$ K for the $x = 0.4 - 0.6$ samples, each offset for clarity. Dashed lines show a slope of 1. Linear behavior in the low-fluence regime is an indication that the optically accessed excitations are fully gapped, as described in the text. (b) The absolute value of the maximum change in reflectivity versus both Φ and the average energy absorbed within a penetration depth for the $x = 0.4$ sample. The red curve is a fit to a simple saturation model yielding $\Phi_{\rm sat} = 25$ μJ/cm^2 at an initial temperature of 7 K.

the sample, given by

$$\Delta R(0)/\Delta R_{\rm sat} = \lambda^{-1} \int e^{-z/\lambda}(1 - e^{-\Phi(z)/\Phi_{\rm sat}})dz, \quad (1)$$

where $\Phi(z) = \Phi(0)e^{-z/\lambda}$ is the laser fluence at a depth of z beneath the sample surface, $\Delta R_{\rm sat}$ is the change in reflectivity at saturation, and λ is the optical penetration depth (26 nm in optimally doped $Ba_{1-x}K_xFe_2As_2$, Ref. 35). The fit yields a saturation fluence of $\Phi_{\rm sat} = 25$ μJ/cm^2 and $\Delta R_{\rm sat}/R = 1.34 \times 10^{-3}$. Below, we restrict our analysis to $\Phi < 2.5$ μJ/cm^2, which is clearly in the linear range of Fig. 4(b) for all three dopings.

In the low-excitation regime, the dynamics of the photoinduced quasiparticles may be understood within the framework of the Rothwarf-Taylor model. This phenomenological model was originally developed to describe nonequilibrium quasiparticle recombination in tunneling experiments.[30] Here, the coupled recovery of a nonequilibrium concentration of quasiparticles n and their binding boson N may be described by the rate equations

$$\dot{n} = I_{\rm qp} + 2\gamma_{\rm pc}N - Bn^2, \quad (2)$$

$$\dot{N} = I_{\rm ph} + Bn^2/2 - \gamma_{\rm pc}N - (N - N_{\rm eq})\gamma_{\rm esc}, \quad (3)$$

where $I_{\rm qp}$ and $I_{\rm ph}$ are the external quasiparticle and boson generation rates, respectively, $\gamma_{\rm pc}$ is the pair creation rate via annihilation of gap energy bosons, $N_{\rm eq}$ is the equilibrium boson number density, $\gamma_{\rm esc}$ is the boson escape rate, and B is the bimolecular recombination constant. The rates Bn, $\gamma_{\rm pc}$, and $\gamma_{\rm esc}$ describe the three different relaxation pathways for the energy deposited into the system by the ultrashort pulse.

Depending on the relative magnitudes of these three rates, the solutions of these equations display different characteristics. In the simplest case, if $\gamma_{\rm pc} \ll Bn$ or $\gamma_{\rm esc} \gg \gamma_{\rm pc}$ then the pair creation term in the first equation can be ignored and the two equations decouple. In this limit, quasiparticles display simple bimolecular kinetics governed by the recombination coefficient B, as is observed, e.g., in Figs. 2(a)–2(c). In the limit where $\gamma_{\rm esc} \ll \gamma_{\rm pc}, Bn$, quasiparticles and bosons come to a quasiequilibrium and the combined population decays with a slow rate proportional to $\gamma_{\rm esc}$. This regime, known as the phonon bottleneck, is consistent with the slow component of the signal, shown in Fig. 3(a).

In the decoupled regime, the RT equations permit determination of the thermal decay rate of quasiparticles ($\gamma_{\rm th}$) and the recombination coefficient B.[20] This may be seen by explicitly drawing a distinction between photoinduced quasiparticles ($n_{\rm ph}$) and thermally present ones ($n_{\rm th}$) and rewriting $n = n_{\rm ph} + n_{\rm th}$. Equation (2) then becomes

$$dn/dt = -Bn_{\rm ph}^2 - 2Bn_{\rm ph}n_{\rm th}, \quad (4)$$

where the second term $Bn_{\rm ph}n_{\rm th}$ represents the recombination of photoinduced quasiparticles with their thermally populated counterparts. We consider the initial recombination rate γ_{r0}, defined as

$$\gamma_{r0} = -(1/n_{\rm ph})(dn_{\rm ph}/dt)|_{t\to 0}, \quad (5)$$

$$= Bn_{\rm ph} + 2Bn_{\rm th} = \gamma_{\rm ph} + 2\gamma_{\rm th}, \quad (6)$$

where $\gamma_{\rm ph,th} = Bn_{\rm ph,th}$ are the photoinduced and thermal decay rates.

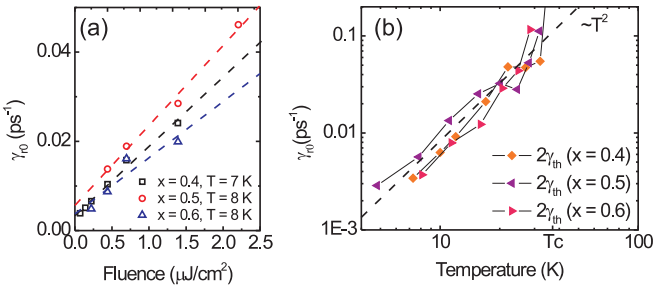

FIG. 5. (Color online) Decay-rate analysis of data with a view toward gap symmetry. (a) The initial decay rate (γ_{r0}) as a function of pump fluence at 7, 8 K for $x = 0.4 - 0.6$. The linear dependence of recombination rate on initial population is a hallmark of bimolecular recombination. Dashed lines show linear fits to data. The thermal decay rate at each temperature was obtain by extrapolating the fits to zero fluence. There is little significant difference between the various dopings. (b) The thermal relaxation rate $\gamma_{\rm th}$ plotted as a function of temperature for $x = 0.4 - 0.6$. The dashed line shows $\sim T^2$ dependence as a guide along for all doping levels, suggesting a negligible change in Fermi surface topology between differently doped samples.

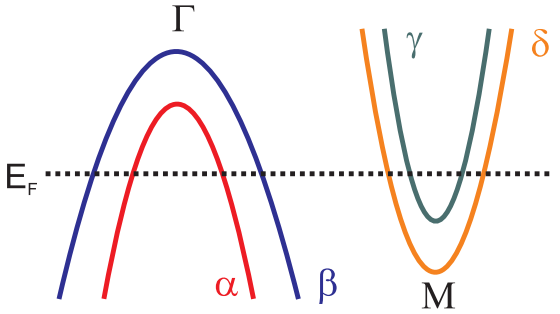

FIG. 6. (Color online) Schematic representation of the pnictide band structure. While five bands have been observed by ARPES, the inner hole band is nearly doubly degenerate and so is represented by the single band α.

Experimentally, we deduce γ_{r0} from the initial slope of the reflectivity transients following the peak. As suggested by Eq. (6), we obtain $\gamma_{\rm th}$ by extrapolating the linear fits to zero excitation density (i.e., $n_{\rm ph} \propto \Phi \to 0$) for each temperature, as shown in Fig. 5(a) at 7 and 8 K. The slope of the fits is proportional to B, which we observed did not strongly depend on the temperature for any of these samples. The intercept $\gamma_{\rm th}$ was observed to increase with T due to the greater thermal quasiparticle population. We shall examine each quantity in turn.

In order to determine the value of B, an estimate of $n_{\rm ph}$ for a given Φ is required, which we will conveniently pick as the saturation fluence. The average energy density deposited by the pump beam within the penetration depth at saturation is $\Phi_{\rm sat}/\lambda = 9.6$ J/cm^3, using the value for $\Phi_{\rm sat}$ determined above. We compare this value with an estimate based on the assumption that saturation occurs when the quasiparticle system receives an energy comparable to the condensation energy, which we approximate from the BCS theory as $1/2N(E_f)\Delta^2$. Here, $N(E_f)$ is the density of states at the Fermi level and Δ is the superconducting gap energy. Using an average gap size of $\Delta = 10$ meV and $N(E_f) = 7.3$ eV^{-1} per unit cell,[12] we obtain a condensation energy of 0.3 J/cm^3. This value is significantly smaller than the experimentally measured saturation energy of 9.6 J/cm^3. Hence only 3% of the energy goes into creating quasiparticle pairs. Using this value to convert the laser fluence into excitation density, we obtain $B = 2.48 \times 10^{-9}$ cm^3/s. For a BCS superconductor in the dirty limit, B is proportional to the ratio of the electron phonon coupling constant to the density of states at the Fermi energy.[40] In the case of pnictide superconductors with multiple gaps, a detailed theoretical model for the quasiparticle recombination is necessary to further interpret the measured value of B.

Figure 5(b) presents $\gamma_{\rm th}$ as a function of temperature for $x = 0.4 - 0.6$. Significantly, the data presented in this figure reveal that the thermal decay rate $\gamma_{\rm th} = Bn_{\rm th}$ is proportional to T^2 below T_c for these doping levels. This suggests the presence of a node in the gap around which $n_{\rm th} \sim T^2$, as opposed to the exponential dependence expected from an isotropic gap. However, the linear dependence of the magnitude of $\Delta R/R$ on Φ at weak excitation levels [Fig. 4(a)] argues against the presence of nodal quasiparticles, which would lead to $\Delta R/R \propto \Phi^{2/3}$, as discussed above.

The phenomenological consistency of the pump-probe measurements in the doping range $x = 0.4 - 0.6$ indicates that the physics of these materials is consistent with the band-dependent picture we have developed for the $x = 0.4$ material.[27] As this picture is central to our understanding of nonequilibrium quasiparticle dynamics in the pnictides, we briefly summarize it using the simplified representation of a pnictide band structure in Fig. 6.

LDA calculations[29] have shown a lack of states 1.5 eV above and (accounting for renormalization[14]) below the Fermi level at the M point of the Brillouin zone, implying that the probe wavelength used in these experiments is not able to couple to quasiparticle dynamics at this location in the zone. This point is bolstered by an estimate of the Sommerfeld parameter, which shows the density of states of the hole bands to be several times larger than at the electron pockets,[12] resulting in a much greater number of photoinduced quasiparticles at the hole pockets as compared with the electron pockets.

Thus, the electron bands γ,δ do not contribute significantly to signal, i.e., $\Delta R(t)/R$ derives almost exclusively from the hole bands. In particular, strong coupling between the carriers in the α bands with those in γ,δ[14,28] leads to the observed excitation-density-dependent dynamics, while the isolation of carriers in β from the other bands is represented by their slow, bottlenecked decay. Furthermore, since the entirety of the signal is due to the hole bands, we may thus interpret the observation $\Delta R(0)/R \propto \Phi$ to indicate that it is these bands which possess fully gapped excitations.

As the excitation density is lowered, the thermal quasiparticle population becomes comparable to, and then exceeds, the photoinduced one. Nonequilibrium quasiparticle recombination is then dominated by the second term in Eq. (4), which represents a photoinduced quasiparticle recombining with a thermal one. This measurement thus becomes particularly sensitive to the presence of either a highly anisotropic gap or a node on the Fermi surface, as the locally small gap energy leads to a relatively higher concentration of thermal quasiparticles in its vicinity.

Here, the observation that $\gamma_{\rm th} \propto T^2$ may be indicative of either a highly anisotropic gap or node on the electron pockets, as interband scattering may be dominated by photoexcited carriers in α recombining with a relatively large population of thermally present carriers in γ,δ. This scenario is compatible with an $s_{\pm}$ order parameter with impurity scattering to account for the T^2 behavior, although it does not require it. The fact that $\gamma_{\rm th} \propto T^2$ does not change up to doping levels of $x = 0.6$ suggests that the Fermi surface topology is consistent up to this doping.

B. $Ba_{1-x}K_xFe_2As_2$: The high-fluence regime

We now shift our attention to phenomena that require a different framework than that developed above, i.e., the observation of coherent oscillations in all samples at the highest fluences ($\Phi > 10\ \mu J/cm^2$) and the dynamics of the underdoped hole-doped samples where $x = 0.2,0.3$.

At fluences greater than $10\ \mu J/cm^2$, we observe the onset of highly damped oscillations in the short time transients shown in Figs. 2(b) and 2(c) that become more apparent with increasing fluence. A clearer depiction of this effect is provided in Fig. 7 by extending the measurement window for the $x = 0.4$ sample. These oscillations are due to stimulated Brillouin scattering,[39] where interference between the portion of the probe beam reflected from the sample surface and from the propagating strain pulse launched by the pump modulates the signal in the time domain. The observed period of ~40 ps is consistent with the expected value of $\lambda_{\rm pr}/(2n v_s \cos\theta)$,[39] where $\lambda_{\rm pr}$ is the wavelength of the probe, θ the angle of incidence, v_s the speed of sound,[41] and n the refractive index. The fast damping rate Γ is set by the small optical penetration depth of the light ($\Gamma = v_s/\lambda$).

The strength of the SBS signal is linearly proportional to the thermal expansion coefficient. Thus the disappearance of the oscillations in the low-fluence data below T_c is a manifestation of its large drop at the transition temperature T_c for all Ba-122 pnictides. This drop is due to the thermodynamic relationship between $c_p(T)$ and the expansivity[31–33] and is more pronounced for expansion along the c axis as a result

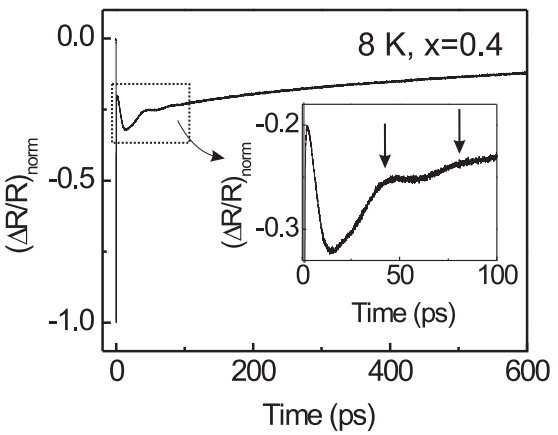

FIG. 7. Dynamics of the decay measured for a longer time window at $T = 8$ K and $\Phi = 37\ \mu J/cm^2$. Highly damped oscillations are observed with a period of ~40 ps (inset).

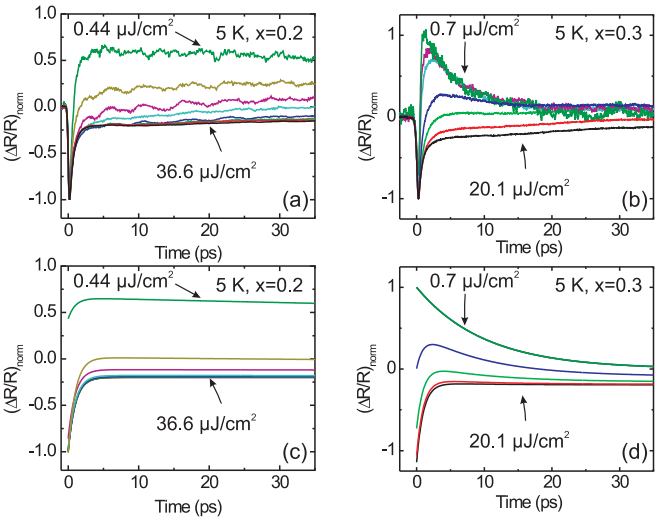

FIG. 8. (Color online) Raw traces in the underdoped hole-doped samples $Ba_{1-x}K_xFe_2As_2$ for (a) $x = 0.2$ ($T_c = 22$ K, $T_{\rm SDW} \sim 100$ K) and (b) $x = 0.3$ ($T_c = 22$ K) at $T = 5$ K. The absorbed fluences are Φ = 36.6 (black – (a) only), 20.1, 12.7, 7.0, 4.4, 2.2, 1.4, and 0.7 (blue) $\mu J/cm^2$. Also shown are simulated results for $\Delta R(t)/R$ at various values of Φ using a simple two-component model in the (c) $x = 0.2$ sample and the (d) $x = 0.3$ sample at the same fluences. The simulations, which are performed without free parameters, show excellent qualitative agreement with the data.

of the layered nature of the pnictides.[33] The presence of an acoustic wave may be an indication that the sample has been partially driven into the normal state, even at the relatively modest fluences used here ($\leqslant 37\ \mu J/cm^2$).

We examine the plausibility of this scenario by simple energy-conservation arguments. We recall that the experimentally measured saturation energy, estimated above as $9.6\ J/cm^3$, supports the hypothesis that high fluences deplete the superconducting condensate. However, this also indicates that a large fraction of the energy deposited by the laser is transferred into other internal degrees of freedom or is carried out of the probed region by through-plane transport of the excited electrons due to, e.g., the large excitation gradient of the pump driving fast diffusion of the excited carriers.

Shifting focus to the underdoped samples, Figs. 8(a) and 8(b) show the $T = 5$ K reflectivity transients in the $x = 0.2$ and $x = 0.3$ samples. In the $x = 0.2$ material, $T_c = 22$ K and a spin-density wave transition occurs at $T_{\rm SDW} = 120$ K. In the $x = 0.3$ sample, $T_{\rm SDW}$ is suppressed to 100 K and T_c is elevated to 32 K.[38] The dynamics observed here are markedly different than those of the optimally and overdoped samples. In the $x = 0.2$ compound, the high-fluence traces resemble the normal state of the $x = 0.4 - 0.6$ samples. With reduced fluence we see the emergence of an intensity-independent, slowly-decaying positive component reminiscent of the slow dynamics of Fig. 3(a).

The dynamics of the $x = 0.3$ sample shown in Fig. 8 reveal behavior similar to those of the $x = 0.2$ sample at the highest fluences, again in contrast with the measurements of Figs. 2(a)–2(c). Here, we observe that with a reduction of the incident laser fluence, a positive component of the signal

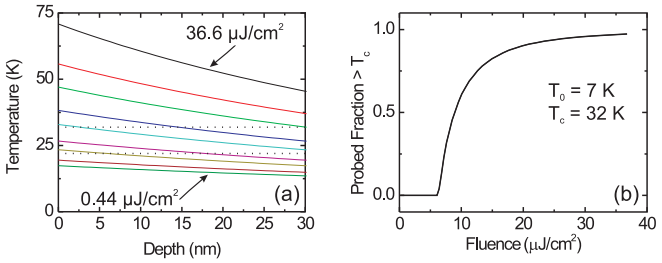

FIG. 9. (Color online) (a) Simulated temperature profile as a function of depth for the fluences used in this study. The dotted lines indicate the values of transition temperature for the $x = 0.2$ ($T_c = 22$ K) and the $x = 0.3$ ($T_c = 32$ K) samples. (b) Fraction of the sample heated into the normal state as interrogated by the penetration depth of the probe for the $x = 0.3$ sample.

emerges whose recovery dynamics are intensity independent and decay on the relatively quick ∼10 ps timescale.

The absence of a bimolecular intensity dependence may be interpreted within the framework of the Rothwarf-Taylor equations as a bottlenecked recombination. Unfortunately, this precludes an analysis to determine gap symmetry. However, we may understand these data by applying a simple model which considers the quasi-equilibrium temperature of the sample $T(z)$ as a function of depth in the sample z after excitation, the results of which are shown in Figs. 8(c) and 8(d). Conservation of energy provides an expression for $T(z)$:

$$\frac{\Phi}{d}\exp(-z/d) = \int_{T_0}^{T(z)} c_p(T)dT. \tag{7}$$

Here, the specific heat $c_p(T)$ was modelled as a fifth-order polynomial using published data on the $x = 0.4$ compound.[42] Equation (7) was then integrated and inverted numerically to reproduce the initial temperature profile, depicted in Fig. 9(a). We note that high fluences produce a significant increase in temperature. In contrast, this increase is very modest at the low fluences examined in Sec. III A.

The pump-probe measurement is an integrated measurement in depth. We therefore calculate the fraction A of the sample which has been brought above the transition temperature from,

$$A = \frac{\int_0^\infty \Theta(z')\exp(-2z'/d)dz'}{\int_0^\infty \exp(-2z'/d)dz'} \tag{8}$$

where $\Theta(z') = 1$ if $T(z') \geqslant T_c$ and $= 0$ otherwise. The factor of 2 in the above equation accounts for the reflection of the beam back through the sample. In practice, this integral was numerically evaluated to three penetration depths. The result is shown in Fig. 9(b). For an initial temperature of 7 K, the entire sample remains below T_c for $\Phi < 6$ μJ/cm^2 and achieves a 90:10 distribution between the normal and superconducting state at $\Phi = 19.8$ μJ/cm^2. The small discrepancy between the value obtained from this simple model and the experimentally measured saturation fluence may be due to the through-plane electronic diffusion mentioned above.

We consider the signal to comprise two parts. The first is a fast-decaying negative component of time scale τ_f with an offset c as $f(t) = -[\exp(-t/\tau_f) + c]$ to represent the normal state contribution. The second is a slow, positive component for the superconducting contribution of time scale τ_s as $s(t) = \exp(-t/\tau_s)$. The two components are then added in the proportion $Af(t) + (1 - A)s(t)$, where the coefficient A is defined as the fraction of the sample seen by the probe beam with $T(z) > T_c$. Here, we compute A as a weighted average of the temperature, as in Eq. (8).

The results of this calculation using $c = 0.2$, $\tau_f = 1$ ps, and $\tau_s = 400$ ps are shown in Fig. 8(c) for the $x = 0.2$ sample. Figure 8(d) uses the same vales for c and τ_f but a value of $\tau_s = 10$ ps for the $x = 0.3$. In both cases, we observe excellent qualitative agreement between the experimental data and the model using no fitted parameters. Data acquired at higher initial temperatures showed similar agreement with this model for both $x = 0.2$ and $x = 0.3$.

We note that this model is not able to replicate the dynamics of the optimally doped and overdoped samples discussed in the previous section. Even when accounting for the change in sign of the phenomenological superconducting component $s(t)$ from positive to negative, no combination of simulation parameters can produce an initial decay rate that depends linearly on excitation fluence. This provides further evidence that the intensity dependence observed in the $x = 0.4 - 0.6$ samples arises from bimolecular recombination kinetics. We thus emphasize that this analysis has no impact on the analysis performed in the low-fluence regime. First, in those traces we deduced the gap symmetry from the initial quasiparticle decay rate γ_0, which was obtained from the slope of the reflectivity transients immediately after the peak, i.e., $t < 1$ ps. This is much shorter than the time required for an equilibrium temperature to be established between the electronic system and the phonons. Second, all the data used in the analysis of Sec. III A were at such low fluences that the simulated equilibrium sample temperature did not depart significantly from the initial value.

The physical processes at play in the $x = 0.2$ and $x = 0.3$ samples may also be understood within the framework of the band-dependent dynamics discussed in the previous section. Ultrafast measurements on the $Ba_{1-x}K_xFe_2As_2$ samples for values of $x < 0.3$ indicate a competition for itinerant electrons between the SDW state and the superconducting state.[25] This observation is consistent with ARPES measurements on $Ba_{0.75}K_{0.25}Fe_2As_2$ which have shown that the superconducting fraction in α and γ,δ are suppressed due to their contribution to SDW order via Fermi surface nesting.[43] At $x = 0.2$ this nesting is even slightly more favored, and hence the bulk of the optical pump-probe response in the superconducting state arises from the slow, intensity-independent decay in the outer hole band β with little to no contribution to the signal from the other bands.

In the $x = 0.3$ sample, the absence of intensity dependence is again due to the presence of a SDW state between α and γ,δ which competes with superconductivity for carriers in these bands. It is, however, unclear at present why the dynamics change from slow to fast at this particular doping.

The presence of a pseudogap state in the 1111 system has already been argued for based on ultrafast pump-probe measurements;[24] ARPES[43] and optical conductivity[44] have indicated the same for underdoped $Ba_{1-x}K_xFe_2As_2$ samples. In the context of the intensity-dependent dynamics studied

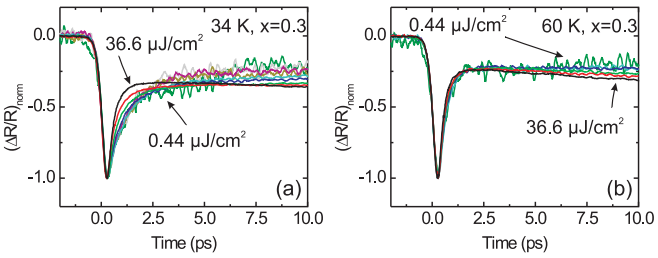

FIG. 10. (Color online) Raw traces in the underdoped hole-doped pnictide $Ba_{0.7}K_{0.3}Fe_2As_2$ ($T_c = 32$ K) above T_c. In (a) we note that there is some residual intensity dependence of the signal, where the initial recovery of the fast component is quicker at the highest fluences than at lower ones. This is identical to the superconducting state, despite the fact that at $T = 34$ K, the sample is in the normal state and the SDW state does not exhibit intensity-dependent recombination (see below). After the initial electronic recovery, the amplitude of the acoustic wave is diminished at lower fluences. (b) In contrast, the fluence dependence of the electronic recovery has all but disappeared at 60 K. In both plots the absorbed fluences are $\Phi = 36.6$, 20.1, 12.7, 7.0, 4.4, 2.2, 1.4, 0.7, and 0.44 μJ/cm^2.

here, pseudogap behavior is suggested by the intensity dependence present above T_c in Fig. 3(c) of Ref. 27 for $x = 0.4$. A clearer demonstration of such fluence dependence is depicted in the time-resolved reflectivity transients of Fig. 10(a), which were measured in the $x = 0.3$ sample 2 K above the transition temperature. There is a discernable tendency toward faster initial relaxation of the reflectivity transients with an increase in temperature. This disappears by 60 K, as may be seen in Fig. 10(b).

In light of the band-dependent relaxation dynamics discussed above, we posit that those carriers participating in the pseudogap state must derive from the α band because these carriers give rise to intensity-dependent recombination in the superconducting state. This conclusion is consistent with prior ARPES measurements on $Ba_{0.75}K_{0.25}Fe_2As_2$ which show the presence of a pseudogap in α but not in the other bands.[43]

C. $BaFe_{2-y}Co_yAs_2$

We now shift our focus to the electron-doped side of the phase diagram. Figure 11(a) depicts the qualitative effect of doping on the Fermi level. As electrons are added to the system, the Fermi level rises in a rigid band manner, as has been observed by Brouet *et al.*[45] At a Co doping of $y = 0.15$, the α band begins to submerge below the Fermi level at various points along k_z.[46] By the point of optimal Co doping at $y = 0.20$, α has been submerged well below the Fermi level.

The reflectivity transients of Fig. 11 exhibit the consequences of the disappearance of α. As a point of comparison, Fig. 11(b) shows data from the parent compound taken at 20 K, well below the SDW transition temperature $T_{SDW} = 143$ K. None of the intensity-dependent relaxation dynamics associated with the $x > 0.4$ hole-doped samples were observed in the undoped sample. We note the small effect of the suppression of the thermal expansion predominantly along the c axis[31–33] which inhibits the generation of an acoustic wave. Qualitatively identical behavior was observed in an

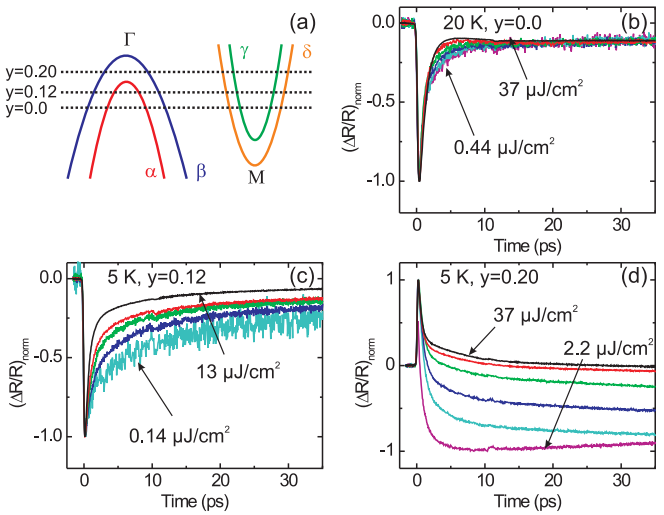

FIG. 11. (Color online) (a) Schematic representation of the band structure of the Ba-122 pnictides. Although this is somewhat of a simplification that ignores the change in k_z dependence with doping,[47] the predominant effect is a shift of the Fermi level up with the addition of electrons:[45] in the parent compound, α and γ,δ nest, leading to SDW behavior. In the underdoped regime ($y = 0.12$), α does not nest appreciably with γ,δ. With the addition of more holes, the α band is submerged below the Fermi level when the doping reaches $y = 0.15$, as measured by Sekiba *et al.*[46] (b) Raw $(\Delta R/R)_{\rm norm}$ traces for the parent compound at 20 K. The moderate amount of intensity dependence in these traces at short times is due to acoustic suppression from the diminished thermal expansion parameter at lower temperatures/fluences. (c) Reflectivity transients in the underdoped sample ($y = 0.12$, $T_c = 12$ K) show a mild amount of intensity dependence of the faster relaxation with increasing fluence, similar to that seen in the hole-doped samples. (d) Fluence dependence of the optimally doped sample ($y = 0.2$, $T_c = 22.5$ K) indicates entirely different relaxation dynamics with fluence. While there appears to be intensity dependence present here, the slope of the initial transient γ_0 is identical for all fluences. The differences between the various fluences and the origin of this nonuniformity of the relaxation dynamics are due to a temperature effect, as described in the text.

underdoped sample ($y = 0.08$, not shown) for which the SDW transition is suppressed to 95 K but which does not superconduct at low temperatures.

Figure 11(c) shows raw data for $BaFe_{1.88}Co_{0.12}As_2$ ($T_c = 12$ K) taken at different fluences ranging from 0.14 to 13 μJ/cm^2. As with the $x = 0.4 - 0.6$ samples, we observe a fast intensity dependence of the signal at short times with higher laser intensities corresponding to faster initial recombination rates. We note that the relatively low $T_c = 12$ K of the $y = 0.08$ sample does not allow us to use the initial decay-rate analysis employed above to determine Fermi surface topology.

With the submergence of the inner hole band α at $y = 0.15$,[46] the characteristics of $(\Delta R/R)_{\rm norm}$ change markedly. Although qualitatively similar behavior was observed in the $y = 0.16$ ($T_c = 16$ K) sample, these dynamics are most clearly represented by the $y = 0.20$ sample due to its slightly higher $T_c = 22$ K. As may be seen in Fig. 11(d), $\Delta R/R$ traces scaled to the initial electronic response at $t = 0$ are qualitatively

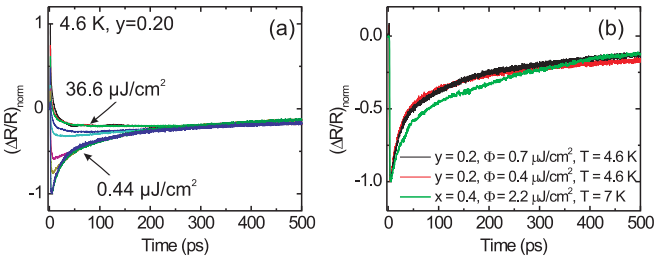

FIG. 12. (Color online) Evolution of $(\Delta R/R)_{\rm norm}$ in $BaFe_{1.8}Co_{0.2}As_2$ for absorbed fluences of $\Phi = 36.6$ (black), 20.1, 12.7, 7.0, 4.4, 2.2, 1.4, 0.7, and 0.44 (blue) μJ/cm^2. As the fluence is increased, the recovery to equilibrium seems to slow due to a greater fraction of the probed sample being heated above T_c, especially at these long time scales. Proper scaling of the various traces yields a common, bottlenecked decay, reached by the sample when the entire probed region has cooled below T_c due to thermal diffusion. (b) Comparison of long-time traces of the optimally hole-doped sample ($Ba_{0.6}K_{0.4}Fe_2As_2$) and the optimally electron-doped ($BaFe_{1.8}Co_{0.2}As_2$) material at fluences of 0.7 and 0.4 μJ/cm^2. Even though the Fermi surface topologies and gap energies of the two samples differ markedly, we note that the relaxation dynamics are nearly identical, indicating a common underlying relaxation mechanism, i.e., bottlenecked quasiparticle recombination in the outer hole band (β). This slow relaxation switches off at the respective values of T_c of both samples.

identical (within a sign) to those of the $x = 0.2$ underdoped hole-doped sample in Fig. 8(a). Indeed, we observe that the polarity of the signal has changed from the underdoped to the optimally doped side of the phase diagram. A similar effect has also been observed in the $Bi_2Sr_2Ca_{1-y}Dy_yCu_2O_{8+d}$ (BSCCO) system of cuprate superconductors.[48]

In order to better interpret the dynamics of Fig. 11(d), we modelled the heat flow out of the excited region after the establishment of an initial equilibrium temperature. This was done by numerically solving the heat-diffusion equation using literature temperature-dependent thermal conductivity[36] and heat-capacity[42] data while assuming a temperature-independent density. The initial condition was specified using Eq. (7) and the incident fluence. In the limit of bottlenecked recombination, $\Delta R(t)/R$ should be independent of initial quasiparticle density once the entire probed region is below T_c. This indicates that the data should be scaled at the time t when the entire sample becomes superconducting.

Reflectivity transients were acquired out to 600 ps and then rescaled at the point in time at which the entire probed depth is below T_c. This rescaling is shown in Fig. 12(a), where we observe a remarkable convergence of the data at long times. The highest fluences measured produce the normal state response, i.e., an initial "spike" followed by a quasi-steady state that does not decay within the time window. As the excitation fluence is reduced, the initial recovery gradually transitions to bottlenecked quasiparticle recombination at earlier and earlier times. At the lowest fluences ($\Phi = 0.72$ and 0.44 μJ/cm^2), the entire probed region is below T_c and there is an intensity-independent, bottlenecked relaxation of the signal.

This behavior recalls the slow dynamics of the optimally hole-doped sample shown in Fig. 3(a). A comparison of these two data sets is provided in Fig. 12(b), which plots data from the optimally hole-doped sample ($x = 0.4$) at $\Phi = 2.2$ μJ/cm^2 alongside data recorded at the lowest fluences in the optimally electron-doped sample ($y = 0.2$). We observe nearly identical behavior, suggesting that these decays arise from the same set of dynamics. As mentioned above, this slow decay was observed to switch off in both samples abruptly at their respective superconducting transition temperatures, indicating that it originates from superconductivity.

We posit that the similarities between the long-time reflectivity transients produced by $Ba_{0.6}K_{0.4}Fe_2As_2$ and $BaFe_{1.8}Co_{0.2}As_2$ may also account for the differences between the data in Figs. 11(c) and 11(d). That is, the disappearance of bimolecular recombination with the doping of electrons derives from the band-dependent recombination dynamics presented above in Sec. III A. The addition of electrons disrupts the near-perfect nesting of α with γ,δ, weakening the effect of the magnetic resonance on Cooper pairing and resulting in a diminished intensity dependence of the $y = 0.12$ sample of Fig. 11(c). Further doping of electrons leads to the submergence of α and thus the remaining relaxation in the $y = 0.20$ sample is the slow decay of photoinduced carriers in β.

IV. SUMMARY AND CONCLUSION

We have presented an ultrafast pump-probe study of the Ba-122 pnictides as a function of fluence and doping on both sides of the phase diagram that provides evidence for band-dependent dynamics. For optimally doped $Ba_{1-x}K_xFe_2As_2$, the initial recovery rate of the reflectivity transients depends linearly on the incident laser fluence Φ in the low-excitation limit. This component of the signal was argued to derive from the inner hole band α. A Rothwarf-Taylor analysis of this intensity dependence in the low-fluence limit yields a T^2 behavior for the thermal population of quasiparticles. At long times, $\Delta R/R$ tended toward a slow, intensity-independent decay which originates from the outer hole band β. These observations were unchanged with an increase of K-doping up to levels of $x = 0.6$. Our results thus indicate fully gapped hole bands with nodal or strongly anisotropic electron bands in these samples.

In underdoped samples ($x = 0.2$,0.3), the intensity dependence disappears as electrons in α are taken up by SDW ordering and hence are unable to participate in superconductivity. The fluence dependence of $\Delta R(t)/R$ is then governed by the decay in β in a proportion which may be estimated by considering the fraction of the probed depth which is driven above T_c by the pump.

In the $BaFe_{2-y}Co_yAs_2$ samples, we observed intensity-dependent recombination at low doping levels ($y = 0.12$) which completely disappeared with the submergence of the inner hole band α by the doping of electrons. The long-time dynamics of these samples were consistent with bottlenecked behavior due to quasiparticle recombination in the outer hole band β.

Intensity dependence was observed to persist above the transition temperature T_c for samples with K doping at levels

of $x \leqslant 0.4$ and was taken as evidence for a pseudogap state. This pseudogap behavior was posited to arise from α, consistent with prior ARPES measurements. No such behavior is observed on the electron-doped side of the phase diagram.

Stimulated Brillouin scattering was observed in all samples above the superconducting transition temperature but disappeared immediately below the transition temperature due to a large decrease of the thermal expansion coefficient at T_c. The presence of Brillouin scattering below the transition temperature for the highest incident fluences used in this study (e.g., $\sim$37 μJ/cm^2) is an indication that even at these relatively modest fluences, the optical pulse was able to bring the sample into the normal state within the penetration depth of the excitation. At the highest fluences, this picture correlated well with basic modeling of reflectivity transients in terms of a linear combination of a normal-state response and a superconducting, bottlenecked quasiparticle recombination, the relative proportions of which are dictated by a simple equilibrium temperature model. In the low-fluence regime, however, where no part of the probed region could reach a temperature greater than T_c, either only bottlenecked or bare bimolecular recombination was observed.

ACKNOWLEDGMENTS

The authors thank B. Andrei Bernevig and Alex Frenzel for useful discussions. This work was supported by DOE Grant No. DE-FG02-08ER46521, the MRSEC Program of the National Science Foundation under Award No. DMR - 0819762, the NSFC, CAS, and the 973 Project of the MOST of China.

*gedik@mit.edu

[1] Y. Kamihara, T. Watanabe, M. Hirano, and H. Hosono, J. Am. Chem. Soc. **130**, 3296 (2008).
[2] M. Rotter, M. Tegel, and D. Johrendt, Phys. Rev. Lett. **101**, 107006 (2008).
[3] M. M. Qazilbash, J. J. Hamlin, R. E. Baumbach, L. Zhang, D. J. Singh, M. B. Maple, and D. N. Basov, Nat. Phys. **5**, 647 (2009).
[4] C. de la Cruz, Q. Huang, J. W. Lynn, J. Li, W. Ratcliff, J. L. Zarestky, H. A. Mook, G. F. Chen, J. L. Luo, N. L. Wang, and P. Dai, Nature **453**, 899 (2008).
[5] Q. Huang, Y. Qiu, W. Bao, M. A. Green, J. W. Lynn, Y. C. Gasparovic, T. Wu, G. Wu, and X. H. Chen, Phys. Rev. Lett. **101**, 257003 (2008).
[6] A. D. Christianson *et al.*, Nature **456**, 930 (2008).
[7] M. D. Lumsden *et al.*, Phys. Rev. Lett. **102**, 107005 (2009).
[8] C. C. Tsuei and J. R. Kirtley, Rev. Mod. Phys. **72**, 969 (2000).
[9] I. I. Mazin, D. J. Singh, M. D. Johannes, and M. H. Du, Phys. Rev. Lett. **101**, 057003 (2008).
[10] F. Wang, H. Zhai, Y. Ran, A. Vishwanath, and D.-H. Lee, Phys. Rev. Lett. **102**, 047005 (2009).
[11] A. V. Chubukov, D. V. Efremov, and I. Eremin, Phys. Rev. B **78**, 134512 (2008).
[12] H. Ding *et al.*, J. Phys.: Condens. Matter **23**, 135701 (2011).
[13] H. Ding *et al.*, Europhys. Lett. **83**, 47001 (2008).
[14] L. Wray *et al.*, Phys. Rev. B **78**, 184508 (2008).
[15] H. Fukazawa *et al.*, J. Phys. Soc. Jpn. **78**, 033704 (2009).
[16] C. Martin *et al.*, Phys. Rev. B **80**, 020501 (2009).
[17] S. Graser *et al.*, New J. Phys. **11**, 025016 (2009).
[18] Y. Yanagi, Y. Yamakawa, and Y. Ono, J. Phys. Soc. Jpn. **77**, 123701 (2008).
[19] W. H. Parker and W. D. Williams, Phys. Rev. Lett. **29**, 924 (1972).
[20] N. Gedik, P. Blake, R. C. Spitzer, J. Orenstein, R. Liang, D. A. Bonn, and W. N. Hardy, Phys. Rev. B **70**, 014504 (2004).
[21] N. Gedik, M. Langner, J. Orenstein, S. Ono, Y. Abe, and Y. Ando, Phys. Rev. Lett. **95**, 117005 (2005).
[22] J. Demsar, R. D. Averitt, A. J. Taylor, V. V. Kabanov, W. N. Kang, H. J. Kim, E. M. Choi, and S. I. Lee, Phys. Rev. Lett. **91**, 267002 (2003).
[23] C. Gadermaier, A. S. Alexandrov, V. V. Kabanov, P. Kusar, T. Mertelj, X. Yao, C. Manzoni, D. Brida, G. Cerullo, and D. Mihailovic, Phys. Rev. Lett. **105**, 257001 (2010).
[24] T. Mertelj, V. V. Kabanov, C. Gadermaier, N. D. Zhigadlo, S. Katrych, J. Karpinski, and D. Mihailovic, Phys. Rev. Lett. **102**, 117002 (2009).
[25] E. E. M. Chia *et al.*, Phys. Rev. Lett. **104**, 027003 (2010).
[26] B. Mansart, D. Boschetto, A. Savoia, F. Rullier-Albenque, A. Forget, D. Colson, A. Rousse, and M. Marsi, Phys. Rev. B **80**, 172504 (2009).
[27] D. H. Torchinsky, G. F. Chen, J. L. Luo, N. L. Wang, and N. Gedik, Phys. Rev. Lett. **105**, 027005 (2010).
[28] P. Richard, T. Sato, K. Nakayama, S. Souma, T. Takahashi, Y. M. Xu, G. F. Chen, J. L. Luo, N. L. Wang, and H. Ding, Phys. Rev. Lett. **102**, 047003 (2009).
[29] F. Ma, Z.-Y. Lu, and T. Xiang, Front. Phys. China **5**(2), 150 (2010).
[30] A. Rothwarf and B. N. Taylor, Phys. Rev. Lett. **19**, 27 (1967).
[31] S. L. Bud'ko, N. Ni, S. Nandi, G. M. Schmiedeshoff, and P. C. Canfield, Phys. Rev. B **79**, 054525 (2009).
[32] F. Hardy, P. Adelmann, T. Wolf, H. v. Löhneysen, and C. Meingast, Phys. Rev. Lett. **102**, 187004 (2009).
[33] M. S. da Luz, J. J. Neumeier, R. K. Bollinger, A. S. Sefat, M. A. McGuire, R. Jin, B. C. Sales, and D. Mandrus, Phys. Rev. B **79**, 214505 (2009).
[34] G. F. Chen, Z. Li, J. Dong, G. Li, W. Z. Hu, X. D. Zhang, X. H. Song, P. Zheng, N. L. Wang, and J. L. Luo, Phys. Rev. B **78**, 224512 (2008).
[35] G. Li, W. Z. Hu, J. Dong, Z. Li, P. Zheng, G. F. Chen, J. L. Luo, and N. L. Wang, Phys. Rev. Lett. **101**, 107004 (2008).
[36] J. G. Checkelsky *et al.*, e-print arXiv:0811.4668.
[37] N. L. Wang (private communication).
[38] H. Chen *et al.*, Europhys. Lett. **85**, 17006 (2009).
[39] C. Thomsen, H. T. Grahn, H. J. Maris, and J. Tauc, Phys. Rev. B **34**, 4129 (1986).
[40] S. B. Kaplan *et al.*, Phys. Rev. B **14**, 4854 (1976).
[41] M. Zbiri, H. Schober, M. R. Johnson, S. Rols, R. Mittal, Y. Su, M. Rotter, and D. Johrendt, Phys. Rev. B **79**, 064511 (2009).

[42]N. Ni, S. L. Budko, A. Kreyssig, S. Nandi, G. E. Rustan, A. I. Goldman, S. Gupta, J. D. Corbett, A. Kracher, and P. C. Canfield, Phys. Rev. B **78**, 014507 (2008).

[43]Y. Xu *et al.*, Nat. Commun. **2**, 392 (2011).

[44]Y. Kwon, J. Hong, Y. Jang, H. Oh, Y. Song, B. Min, T. Iizuka, S. Kimura, A. Balatsky, and Y. Bang, e-print arXiv:1007.3617.

[45]V. Brouet, M. Marsi, B. Mansart, A. Nicolaou, A. Taleb Ibrahimi, P. Le Fèvre, F. Bertran, F. Rullier-Albenque, A. Forget, and D. Colson, Phys. Rev. B **80**, 165115 (2009).

[46]Y. Sekiba, T. Sato, K. Nakayama, K. Terashima, P. Richard, J. H. Bowen, H. Ding, Y.-M. Xu, L. J. Li, G. H. Cao, Z.-A. Xu, and T. Takahashi, New J. Phys. **11**, 025020 (2009).

[47]S. Thirupathaiah, S. de Jong, R. Ovsyannikov, H. A. Dürr, A. Varykhalov, R. Follath, Y. Huang, R. Huisman, M. S. Golden, Y.-Z. Zhang, H. O. Jeschke, R. Valentí, A. Erb, A. Gloskovskii, and J. Fink, Phys. Rev. B **81**, 104512 (2010).

[48]N. Gedik, M. Langner, J. Orenstein, S. Ono, Y. Abe, and Y. Ando, Phys. Rev. Lett. **95**, 117005 (2005).